SAND2023-05226C

Event-based sensing for the detection of modulated signals in degraded visual environments

Christian Pattyn, Alexander Edstrom, Andres Sanchez, Karl Westlake, John van der Laan, et al.

Christian A. Pattyn, Alexander W. Edstrom, Andres L. Sanchez, Karl Westlake, John D. van der Laan, J. Derek Tucker, Jessica Jones, Kaylin Hagopian, Joshua C. Shank, Lilian K. Casias, Jeremy B. Wright, "Event-based sensing for the detection of modulated signals in degraded visual environments," Proc. SPIE 12514, Image Sensing Technologies: Materials, Devices, Systems, and Applications X, 1251409 (15 June 2023); doi: 10.1117/12.2663385

Event: SPIE Defense + Commercial Sensing, 2023, Orlando, Florida, United States

Event-based sensing for the detection of modulated signals in degraded visual environments

Christian A. Pattyn*, Alexander W. Edstrom, Andres L. Sanchez, Karl Westlake,
John D. van der Laan, J. Derek Tucker, Jessica Jones, Kaylin Hagopian, Joshua C. Shank,
Lilian K. Casias, and Jeremy B. Wright

Sandia National Laboratories, P.O. Box 5800, Albuquerque, United States

*capatty@sandia.gov, fog@sandia.gov

ABSTRACT

Event-based sensors are a novel sensing technology which capture the dynamics of a scene via pixel-level change detection. This technology operates with high speed (>10 kHz), low latency (10 μs), low power consumption (<1 W), and high dynamic range (120 dB). Compared to conventional, frame-based architectures that consistently report data for each pixel at a given frame rate, event-based sensor pixels only report data if a change in pixel intensity occurred. This affords the possibility of dramatically reducing the data reported in bandwidth-limited environments (e.g., remote sensing) and thus, the data needed to be processed while still recovering significant events. Degraded visual environments, such as those generated by fog, often hinder situational awareness by decreasing optical resolution and transmission range via random scattering of light. To respond to this challenge, we present the deployment of an event-based sensor in a controlled, experimentally generated, well-characterized degraded visual environment (a fog analogue), for detection of a modulated signal and comparison of data collected from an event-based sensor and from a traditional framing sensor.

Keywords: event-based sensing; degraded visual environments; fog; scattering

1. INTRODUCTION

Degraded visual environments (DVEs) are generally defined as any environment where visibility is impaired. Though many conditions can lead to DVEs, atmospheric phenomena, such as fog, are among the most common. Under these conditions visibility is degraded by obscurant particles (in the case of fog, aerosolized water droplets) which both scatter and absorb light. Attenuation in this manner decreases both the resolution and intensity of optical signals, thereby degrading situational awareness. Ultimately, these effects can have significant impact on sensing infrastructure and cannot be easily overcome. As such, there is continued work to develop and seek out novel solutions which may improve sensing through DVEs[2-8]. In this work we focus on assessing the potential use of event-based sensors (EBSs) in a DVE caused by an experimentally generated atmospheric aerosol analogue.

EBSs are novel focal plane arrays in which each pixel acts independently and asynchronously, generating highly temporally accurate events when changes in the scene are detected. This sensing architecture uses pixel-level analog circuits to detect when the log-intensity of a pixel's incident light has changed by a quantized amount and reports events only in response to changes that exceed a selectable threshold. Using log-intensity rather than intensity enables the high dynamic range (120 dB) seen in these sensors. Due to this novel architecture, some of the benefits of using an EBS compared to a state-of-the-art frame-based sensor include improved temporal resolution (>10 kHz), reduction in data for improved bandwidth transmissions, and lower power consumption (<1 W). Put simply, these effects are achieved because the sensing architecture allows for a significant amount of preprocessing to be performed by the detector, instead of by a postprocessor (i.e., a computer or microcontroller).

It is due to these attributes that we believe EBSs may be advantageous for detecting regularly modulated signals (e.g., an optical chopper rotating at a set frequency, a regularly pulsing light-emitting-diode (LED)) through DVEs when compared

Image Sensing Technologies: Materials, Devices, Systems, and Applications X, edited by Nibir K. Dhar,
Achyut K. Dutta, Sachidananda R. Babu, Proc. of SPIE Vol. 12514, 1251409
© 2023 SPIE · 0277-786X · doi: 10.1117/12.2663385

to traditional framing cameras. We anticipate the preprocessing performed by the detector will allow for simpler isolation of modulated signals in postprocessing as the camera preferentially reports significant events and is less likely to struggle with optical blinding compared to traditional framing cameras. Herein we describe initial experiments and results from deploying an EBS at an atmospheric aerosol testbed.

2. BACKGROUND

Below, we provide some high-level background relevant to the discussions contained within the manuscript. We would like to specifically draw attention to the fact that at present we are comparing our current work and analysis to previous work performed in this space using framing cameras[2, 3, 5, 7-18]. These framing datasets were collected in a variety of different DVEs, some experimentally generated and others naturally occurring. Furthermore, these experiments were typically performed to detect stationary objects within a DVE, not a rotating target as presented in this work. This discrepancy is significant and requires different types of signal analysis (contrast detection instead of frequency detection). Though the experiments differ from one another in this regard, comparing them provides a useful foundation on which to develop further analysis of the two sensing technologies moving forwards (see **Section 6** for our intended future work).

2.1 Event-based sensor architecture

Unlike traditional framing cameras, which report absolute intensity for all pixels at the camera's specific frame rate by scanning each pixel and recording their intensity into a frame, the pixels of an EBS are triggered by a change in illumination of a certain contrast. Biases across the pixel control this contrast threshold and modify the sensitivity of the sensor to contrast changes. This will alter the change in flux needed to trigger a positive (increased flux, or an "ON" event) or negative (decreased flux, or an "OFF" event) reading.

Subsequently, the data stream from an EBS is significantly different than that from a framing camera. **Figure 01** shows the time-space difference between a standard framing camera and an EBS output when both are viewing the same scene (a dot on a disk rotating at various velocities). As mentioned previously, the framing camera reports the intensity for all pixels at the specified frame rate by scanning each pixel. This scanning process is typically slow, leading to motion blur for high-speed objects (**Figure 01**, top). Compression of this data-dense cube is power intensive, thus frame-based imagers are not run continuously in fielded applications where power and/or data exfiltration is limited.

EBSs, on the other hand, will output a continuous stream of events (**Figure 01**, bottom) formatted as a list of 4-tuples ($\{x, y, t, p\}$), encoding the event's pixel x-y coordinate, timestamp, and polarity (indicating an increase or decrease of brightness). If the change is positive (negative), an ON (OFF) event is triggered and the reference intensity level for that pixel is updated. If there are no changes no data are transmitted.

Because EBSs do not necessarily require the assimilation of data from the entire pixel array simultaneously, their temporal resolution can surpass 10 kHz if only a handful of pixels are triggered at any given moment. The output of this architecture is a continuous event data stream which is dense with information regarding changes within a scene but requires less bandwidth and storage space than the data output by a framing camera observing the same scene.

2.2 Light scattering in atmospheric aerosols and the bulk scattering coefficient

Atmospheric aerosols degrade visibility through the scattering and absorption of light. Single scattering or absorption events are well described by Mie scattering theory, which describes the interaction between an electromagnetic plane wave and a scatterer. Mie scattering theory is solved assuming the scatterers are homogenous spheres which are separated enough from one another that the electric fields from scattering events on separate particles do not interfere with one another[19-21]. Because of the effects of surface tension, water droplets suspended in air are approximately spherical, and in a non-turbulent environment it can be assumed they are far enough apart from one another that Mie scattering theory can be applied[3, 5, 8, 15, 22].

Application of Mie theory calculates the scattering and absorption cross sections of an individual droplet as a function of the wavelength of the incident plane wave and the diameter and refractive index of the droplet. We employ a MATLAB code from Mätzler[23] to perform these calculations. As these scattering and absorption effects compound, optical signal decreases in intensity and is spatially blurred[2, 3, 7, 8, 15, 24]. These effects can be integrated for a bulk aerosol through understanding the microphysical characteristics of the aerosol[3, 5, 7, 8, 15, 22, 25] (e.g., droplet size distribution and number

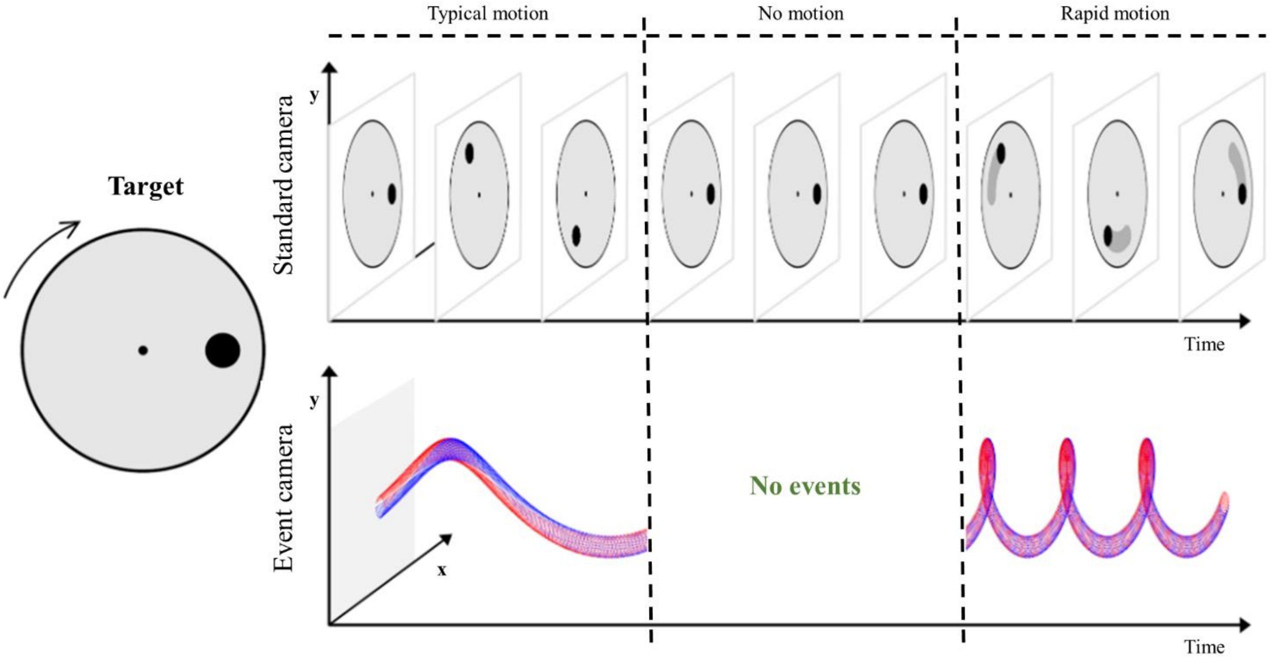

Figure 01. Adapted from Davison, *et al.*[1]. Output of a standard framing camera (top row) and an event-based camera (bottom row) when both are viewing a dot on a disc rotating at varying velocities. Note that event polarity is denoted by red (ON) and blue (OFF).

density). The bulk aerosol scattering coefficient, μ_s (calculated in **Equation 1**, **Section 3.1**) is a useful metric to compare the performance of optical systems in DVEs as it directly relates the optical properties of the DVE to its microphysical properties, thus allowing for the comparison of optical sensing systems via a relevant, physics-informed metric.

2.3 EBS for optical sensing in DVEs

Previous work has been performed to understand and improve the limits of detection for framing cameras in atmospheric aerosols[2, 3, 5, 7-18]. We compare our results to μ_s values presented in the framing sensor literature for the detection and resolution of stationary objects within this DVE (i.e., fog). Again, we would like to point out there lies a fundamental difference between this historical work and our experimentation and analysis to this point – namely, we present the detection of a rotating object's frequency through a DVE, while the cited works focus on the detection of stationary objects. Though this difference is not insignificant, we believe this comparison lays a useful foundation on which to build future discussion on comparing framing and EBS architectures.

EBSs and framing cameras should have similar ultimate limits of detection (i.e., a point at which neither system can recover additional information from light scattered by an atmospheric aerosol) as the underlying physics of the DVE is fundamentally unchanged by the presence of either imaging sensor. However, we expect EBSs will prove to have an advantage over framing sensors for the detection of modulated signals through this DVE. Specifically, we anticipate EBSs may be capable of detecting modulated signals through DVEs with greater computational efficiency than framing cameras. We believe this advantage will be a direct result of the novel EBS architecture down-selecting scene data to pass only changes to the postprocessor. This will directly allow for a greater sample rate, more data transmission over the same amount of bandwidth, and create inherently smaller, less dense datasets than a framing camera.

Finally, the high dynamic range (>120 dB) of the asynchronous pixels in EBSs allows for imaging of scenes in which light intensity varies dramatically (e.g., a scene which is partially in shadow and partially in bright daylight)[26]. We believe this dynamic range may allow for easier isolation of change in DVEs without being blinded by light reflected from a source.

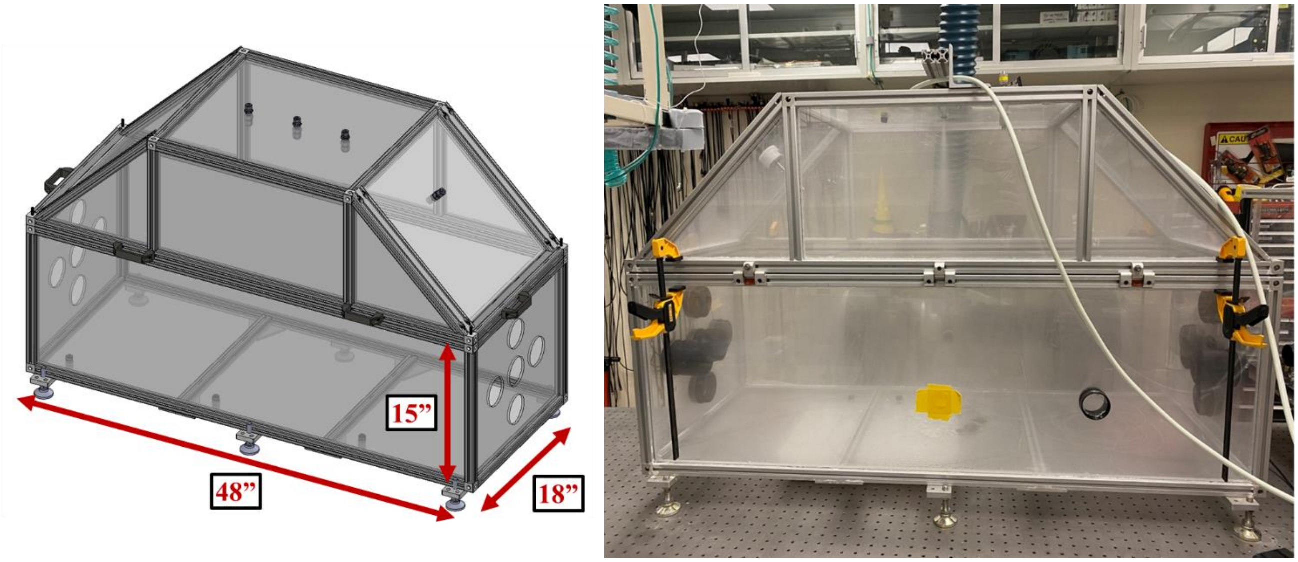

Figure 02. Schematic rendering of the experimental testbed (left) and image of aerosol generation within the fully assembled testbed (right).

3. EXPERIMENTAL SETUP

We utilized the Sandia National Laboratories Tabletop Aerosol Chamber as the testbed for our experimentation. This system is a 48 x 18 x 15-inch acrylic rectangular chamber with a 15-inch-tall trapezoidal head space (pictured in **Figure 02**). The chamber is fit with two sets of five optical windows (stock number 34-528 from Edmund Optics) arranged in parallel from one another across the long axis of the chamber (see **Figure 02**). Each window pair creates a path through which optical measurements can be conveniently taken. Configuration of our optical equipment through these paths can be seen in **Figure 03**.

3.1 Aerosol generation and characterization

Aerosols are generated inside the chamber via an air atomizing spray nozzle (1/4J from Spraying System Co.) placed at the crown of the chamber. The nozzle is connected to an air compressor and a water tank with non-static tubing. When the system is activated water flows from the tank to the nozzle where it is atomized by the air flow, generating an aerosol. This system has been shown to repeatably generate multiple, atmospherically relevant aerosols as a function of the composition of the water flow[5, 22].

The aerosol environment is measured by a Malvern Spraytec, which measures aerosol droplet size distribution, and an in-house multi-band transmissometer, which measures optical transmission through the chamber at 0.532, 1.55, and 9.68 µm. Using these measurements, we can calculate the scattering coefficient of the bulk aerosol using[3, 7, 22]:

$$\mu_s = N \sum_i \sigma_{s_i} n_i , \tag{1}$$

where μ_s is the scattering coefficient of the bulk aerosol in m^{-1}, N is the overall number density of aerosolized droplets in the ambient environment (in cm^{-3}, calculated from the transmissometer measurement), σ_{s_i} is the scattering cross section from Mie theory (in m^2) of a droplet with diameter d_i for light with wavelength λ (calculated for diameters measured by the Malvern Spraytec using MATLAB code from Matzler[23]) and n_i is the relative number fraction of droplets with diameter d_i within the aerosol (measured by the Malvern Spraytec).

The bulk scattering coefficient, μ_s, expresses the attenuation of an optical signal through the bulk aerosol as a function of the microphysical properties of the aerosol. Because of this, it is a convenient metric to compare the performance of optical

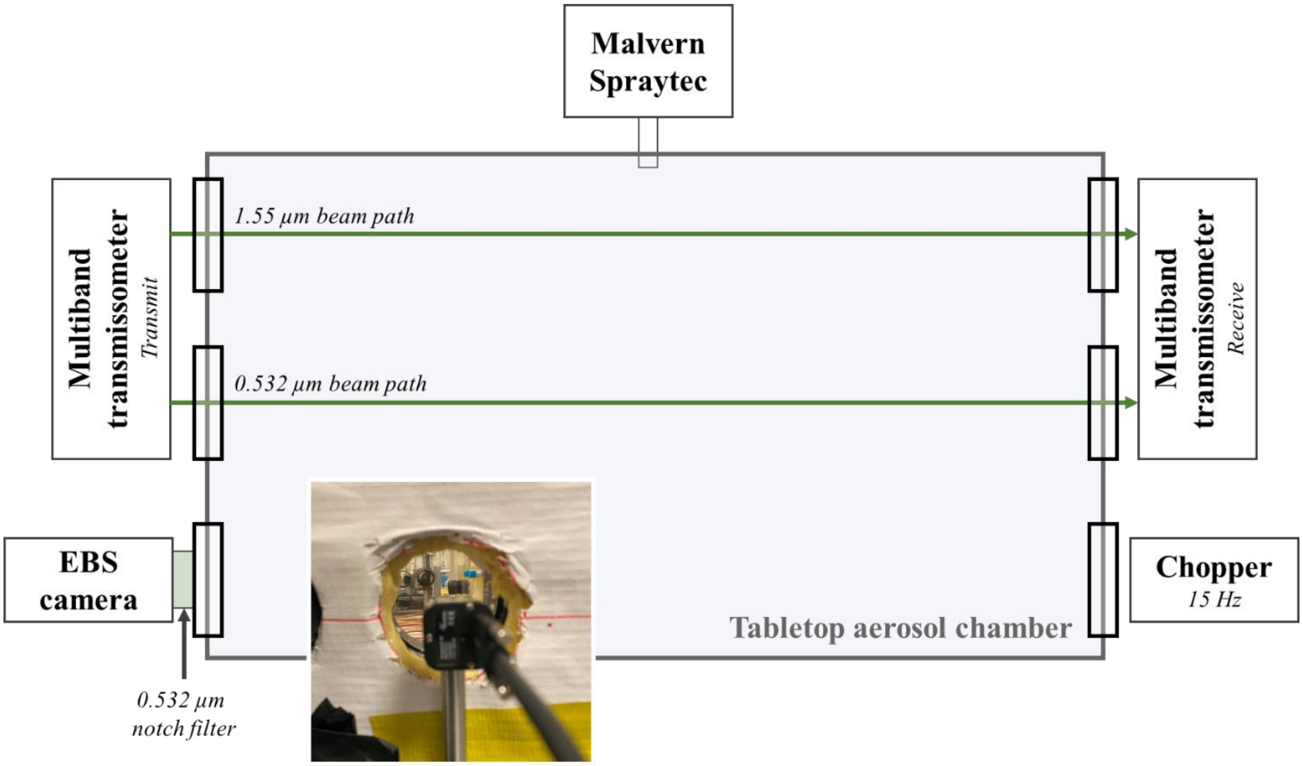

Figure 03. Block flow diagram of the experimental setup. Overlay shows the alignment of the camera (near end) and the rotating optical chopper (far end). The Malvern Spraytec is connected to the chamber via an inhalation cell. The 0.532 and 1.55 µm beams from the multi-band transmissometer are aligned through two optical paths, while the event camera and chopper are aligned along a third path. A 0.532 µm notch filter is placed in front of the camera lens to prevent false signal from scattering of the 0.532 µm transmissometer beam.

systems in DVEs, as system performance can be directly correlated to the optical and microphysical conditions of the environment.

3.2 Event camera and target

EBS data were collected using a third generation SilkyEvCam, EvC3A event camera which uses a model PPS3MVCD Gen3.1 (VGA) EBS from PROPHESEE. The camera was aligned along one optical path to face an optical chopper rotating at 15 Hz placed on the far side of the chamber. The contrast sensitivity threshold biases on the EBS were set to 404 (positive, ON event) and 229 (negative, OFF event). Changing these biases changes the minimum contrast (measured in percentage) required to produce an event[27]. **Figure 03** depicts the arrangement of all equipment with respect to the tabletop aerosol chamber.

3.3 Experimental procedure

Following setup, a baseline measurement was taken with the EBS camera wherein it recorded the chopper for two minutes through the chamber with no aerosol present. Once the baseline measurement had concluded we activated the aerosol generation system and allowed the system to run for five minutes (this procedure can be found in significantly greater detail in Pattyn *et al.*[22]). This created a fog-like aerosol which completely obscured the chopper from the EBS. The aerosol was then allowed to dissipate until the camera signal returned to baseline (a roughly 10-minute period).

4. EVENT DATA PROCESSING AND DETECTION

Two sets of data were collected in the experiment described in **Section 3**: 1) event stream data from the EBS and 2) fog characterization data from the Malvern Spraytec and multi-band transmissometer. EBS data were processed using a time

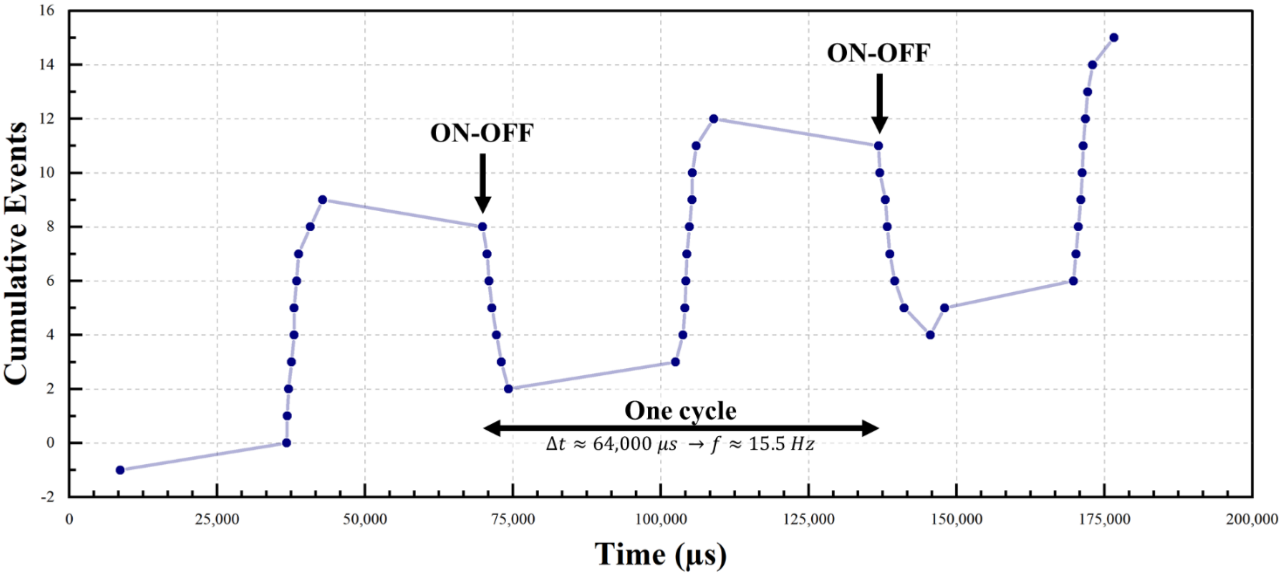

Figure 04. Graphical depiction of cumulative event data on a single pixel over time. Events are indicated by datapoints (circles), positive (ON) events are given a value of +1 while negative (OFF) events are given a value of -1. When an OFF event follows an ON event the timestamp is saved. The next occurrence of this is then compared against the saved timestamp to calculate Δt.

differentiating algorithm developed in-house, described in **Section 4.1**. These data were then time correlated to measured and calculated microphysical and optical properties of the aerosol.

4.1 EBS data processing using a time differentiating (Δt histogram) algorithm

EBS data was processed using an in-house time differentiating (Δt histogram) algorithm. For each time window (e.g., 1 second), this algorithm calculates the time differences (Δt's) between sequential events at each pixel and creates a histogram out of them. To calculate the Δt's, the algorithm can use all events in the pixel's event stream or down select to use positive only, negative only, ON/OFF transitions (when a positive event is followed by a negative event), or OFF/ON transitions. In our application, we are using the Δt's calculated from ON/OFF transmissions. **Figure 04** shows a graphical depiction of cumulative event data on a single pixel over time where events are indicated by datapoints (circles), positive (ON) events are given a value of +1 while negative (OFF) events are given a value of -1. When an ON event follows an OFF event, the timestamp is saved. The next occurrence of this is then compared against the saved timestamp to calculate Δt. Finally, at each time window boundary and for each pixel, the algorithm reports the histogram bin with the maximum counts (peak) and converts the selected Δt into frequency simply using:

$$f \approx \frac{1}{\Delta t}. \tag{2}$$

It repeats the same process for every pixel in each time window, thus generating a spatial distribution on each pixel's detected frequency (an example of which is shown in **Figure 05 (left)**).

This pixel level data is then cumulated into a histogram of reported frequencies over the entire array and is correlated to fog properties using their initial timestamps. This allows us to plot a 3D histogram surface of frequency, count, and aerosol property (**Figure 05 (right)**).

4.2 Definition of detection

To isolate our analysis to the performance of the camera architecture we define detection using an analysis which is naïve to the scene. That is, the detection algorithm does not take into consideration any data acquired during the baseline step (**Section 3.3**). Instead, at each timestep we compared the frequency reported by the highest number of pixels to the frequency reported by the second highest number of pixels. If the most significant frequency was more than three times greater than the next most significant frequency, we considered it to be signal, while all other frequencies were relegated

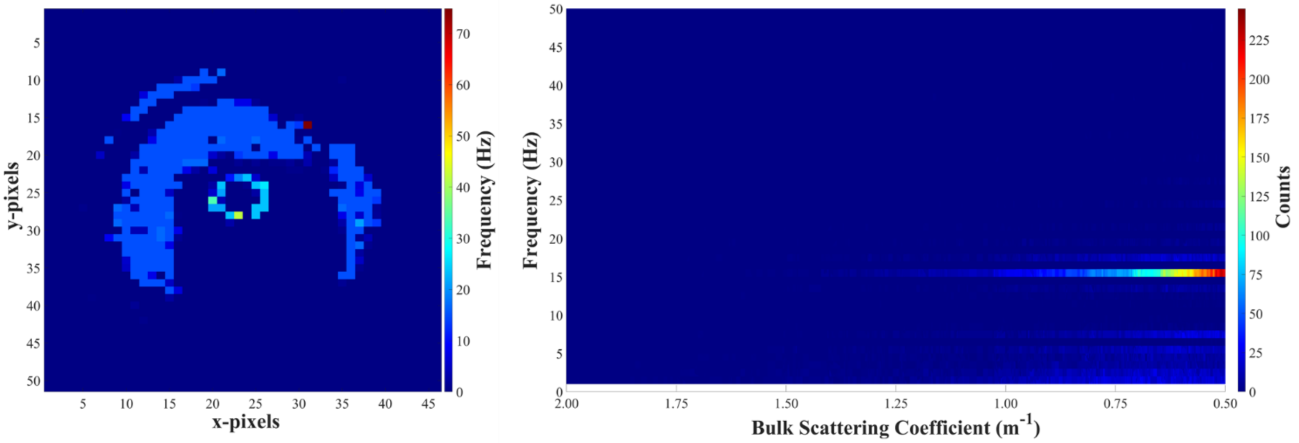

Figure 05. Left: detected frequency mapped to EBS pixel array to create an image of the region of interest containing the optical chopper. Data taken at final timestep of the experiment, correlating to $\mu_s = 0.50$ in the right plot. Right: detected frequency vs. bulk scattering coefficient of the aerosol. Bulk scattering coefficient (x-axis) is presented reversed to correlate more directly with time, that is, as more time passes the aerosol dissipates, decreasing the bulk scattering coefficient.

to noise and non-signals-of-interest. If a signal persisted for more than five consecutive time steps, we considered it a detection.

This approach is intentionally obtuse and meant to isolate only the performance of the sensor architecture by analyzing the output data with simple metrics (though many highly sophisticated algorithms and techniques exist for signal recovery).

5. RESULTS AND DISCUSSION

The Δt histogram algorithm processing of the EBS data successfully detected the 15 Hz signal of interest at $\mu_s = 1.2\ m^{-1}$ (**Figure 05**), or roughly 15% visible transmission through the chamber. **Figure 05 (left)** presents a colormap of the section of the scene where the chopper was present, reconstructed from pixel x-y coordinates (the x- and y-axes, respectively) for the final 1-second time window (correlating to $\mu_s = 0.50$) in the experiment. In this figure, color correlates to the frequency detected at each pixel. The body of the chopper wheel can be visualized by the large patch of light blue (corresponding to a detection frequency of roughly 15 Hz) in the scene. Additional analysis of the scene also shows a ring in the center of the chopper which was rotating at a higher frequency than the rest of the chopper (roughly 22 Hz). Upon investigation the body of the chopper, it was determined that the signal comes from a set of three screws used to mount the wheel to the motor. The chopper itself only had two blades, thus when it was set to 15 Hz the screws in the center triggered detections at 150% the rate of the chopper, or roughly 22 Hz. Detection of this set of frequencies could also be suppressed if foreknowledge of the scene or target of interest was assumed in data processing.

Figure 05 (right) shows the results of the processing steps described in **Section 4.1**, where detected chopper frequency is plotted against the bulk scattering coefficient of the aerosol. The color of each point indicates the number of pixels which reported the given frequency at the given bulk scattering coefficient. It is clear the 15 Hz signal is the dominant signal in the scene. Upon further investigation of the results, many of the other detected signals are harmonics (fractions or multiples) of the 15 Hz signal of interest. Identification and suppression of these signals is one potential way to increase the signal-to-noise ratio of these data.

Finally, **Figure 06** presents the event rate (the number of events detected by the array per half second) and the visible transmission through the aerosol against the full experimental time (~800 seconds, or just over 13 minutes). At current, with the algorithms and definitions discussed in **Section 4** we detect the signal of interest (15 Hz) at ~15% visible transmission (corresponding to the $\mu_s = 1.2\ m^{-1}$ value given earlier in this section). Through analysis of **Figure 06** it can be seen the event rate begins increasing between 5 and 10% visible transmission. This implies that with more rigorous post-processing (i.e., applying denoising / filtering methods) of event data it may be possible to isolate the signal of interest

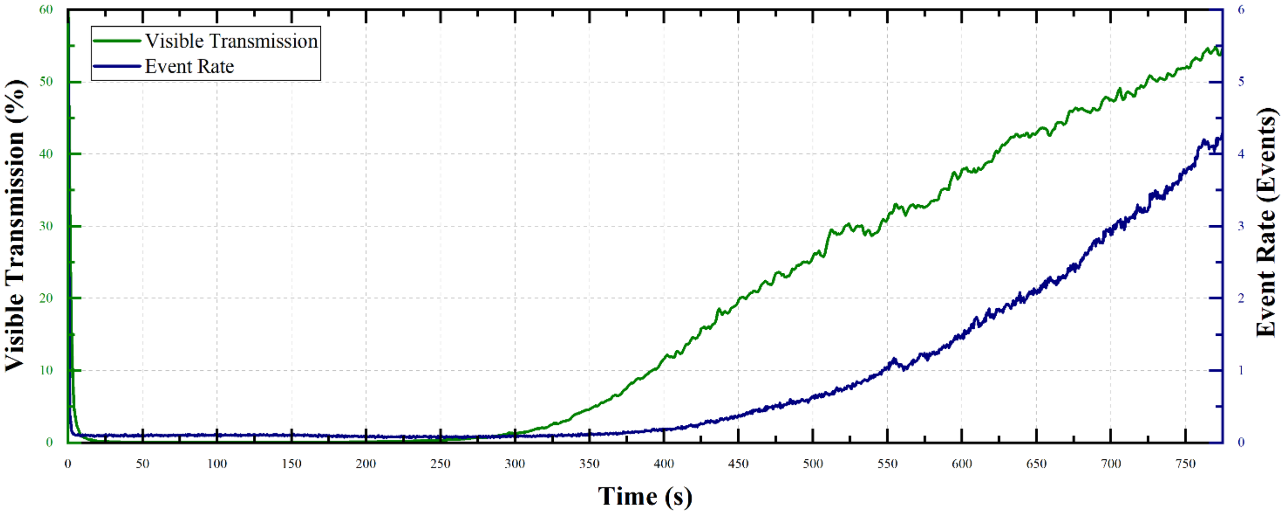

Figure 06. Event rate output when looking at a 15 Hz rotating chopper and visible transmission (as measured by the 0.532 µm path of the multi-band transmissometer). Event rate begins to increase from 5-10% transmission after the aerosol had partially dissipated.

even earlier into the experiment (when the fog is less visibly transmissive - i.e., μ_s is greater). These preliminary results indicate EBS presents a distinct advantage over framing sensors when sensing through fog, and that more sophisticated signal recovery techniques than those presented here can push the limits of detection even further.

6. CONCLUSIONS AND FUTURE WORK

We have presented initial data for the detection of a modulated optical signal through a DVE (created by a fog-like aerosol) using an EBS. Using event stream data, we isolated a modulated signal of interest (an optical chopper rotating at 15 Hz) in an aerosol with a bulk scattering coefficient of $1.2\ m^{-1}$. The novel architecture of the EBS array generated a sparse data stream which allowed for simple isolation and analysis of motion within the scene.

The next step in our work will be to apply a variety of different processing algorithms to data collected using different commercial, off-the-shelf EBS hardware. We will compare processed datasets to one another to develop our understanding of the strengths and weaknesses of each algorithm through fog and understand the frequency detection limitations of each. For instance, we will compare current results to other Δt algorithms, motion segmentation algorithms, and a Lomb-Scargle computational algorithm. In doing so, we will improve understanding of the inherent limitations of these baseline algorithms through fog and will subsequently seek out or develop additional algorithms or filtering methods to isolate events caused by the fog (from phenomena such as light scatter or random aerosol motion).

We will further begin to explore the impact of changing the pixel trigger biases of each set of EBS detectors. By changing the offset biases of each pixel, we can effectively increase or decrease the sensitivity of the entire array. We will investigate how sensitivity affects the ultimate dataset and how these data, combined with the processing algorithms described above, function for the detection of a variety of modulated signals (i.e., a chopper rotating at a higher frequency, a pulsing LED, and an industrial fan) through DVEs in pursuit of optimizing the performance of this system.

Finally, we will investigate the function of these sensors at a greater standoff distance, imitating more relevant scenarios. For this we have begun experimental work at the Sandia National Laboratories Fog Chamber (SNLFC) using fan and LED observables. This chamber is significantly larger than the tabletop aerosol chamber discussed in this research and allows for the generation of aerosols dense enough to imitate distances greater than one kilometer. This larger spatial dimension will allow us to investigate the function of EBS in increasingly relevant real-world environments.

ACKNOWLEDGEMENTS

The authors would like to acknowledge and thank Matthew Tezak, Steven Storch, and Laura Lemieux for their work and contributions to the experiments.

This research was supported by the Laboratory Directed Research and Development (LDRD) Program at Sandia National Laboratories. Sandia National Laboratories is a multimission laboratory managed and operated by National Technology & Engineering Solutions of Sandia, LLC, a wholly owned subsidiary of Honeywell International Inc., for the U.S. Department of Energy's National Nuclear Security Administration under contract DE-NA0003525. This paper describes objective technical results and analysis. Any subjective views or opinions that might be expressed in the paper do not necessarily represent the views of the U.S. Department of Energy or the United States Government.

REFERENCES

[1] Kim, H., Leutenegger, S., and Davison, A. J., "Real-Time 3D Reconstruction and 6-DoF Tracking with an Event Camera," 349-364 (2016).

[2] Duthon, P., Colomb, M., and Bernardin, F., "Light Transmission in Fog: The Influence of Wavelength on the Extinction Coefficient," Applied Sciences, 9(14), (2019).

[3] Bentz, B. Z., Pattyn, C. A., van der Laan, J. D., Redman, B. J., Glen, A., Sanchez, A. L., Westlake, K., and Wright, J. B., "Incorporating the effects of objects in an approximate model of light transport in scattering media," Optics Letters, 47, (2022).

[4] Hastings, R. L., Bentz, B. Z., Lin, D., and Webb, K. J., "Simultaneous Imaging and Localization in a Heavily Scattering Random Medium With Speckle Data From a Moving Object," OSA Technical Digest, STu2F.2 (2021).

[5] Pattyn, C. A., Zenker, J., Deneke, E., Patel, L., Redman, B., van der Laan, J., Hastings, R., Alexander, D., Webb, K., Glen, A., Sanchez, A., Westlake, K., Bentz, B., and Wright, J., "Development and characterization of a tabletop fog chamber at Sandia National Laboratories," 12125 (2022).

[6] Wright, J. B., Laan, J. D. v. d., Westlake, K., Bentz, B. Z., Sanchez, A. L., Glen, A., and Redman, B. J., "Characterizing Fog at the Sandia Fog Facility," Proceedings of SPIE 11424 (2020).

[7] Redman, B. J., and van der Laan, J. D., "Measuring resolution degradation of long-wavelength infrared imagery in fog," Optical Engineering, 58(05), (2019).

[8] van der Laan, J. D., Wright, J. B., Kemme, S. A., and Scrymgeour, D. A., "Superior signal persistence of circularly polarized light in polydisperse, real-world fog environments," Applied Optics, 57(19), 5464-5473 (2018).

[9] Gultepe, I., Müller, M. D., and Boybeyi, Z., "A New Visibility Parameterization for Warm-Fog Applications in Numerical Weather Prediction Models," Journal of Applied Meteorology and Climatology, 45(11), 1469-1480 (2006).

[10] Gultepe, I., Pearson, G., Milbrandt, J. A., Hansen, B., Platnick, S., Taylor, P., Gordon, M., Oakley, J. P., and Cober, S. G., "The Fog Remote Sensing and Modeling Field Project," Bulletin of the American Meteorological Society, 90(3), 341-360 (2009).

[11] Gultepe, I., Tardif, R., Michaelides, S. C., Cermak, J., Bott, A., Bendix, J., Müller, M. D., Pagowski, M., Hansen, B., Ellrod, G., Jacobs, W., Toth, G., and Cober, S. G., "Fog Research: A Review of Past Achievements and Future Perspectives," Pure and Applied Geophysics, 164(6), 1121-1159 (2007).

[12] Ben Dor, B., Devir, A. D., Shaviv, G., Bruscaglioni, P., Donelli, P., and Ismaelli, A., "Atmospheric scattering effect on spatial resolution of imaging systems," Journal of the Optical Society of America A, 14(6), 1329-1337 (1997).

[13] Kopeika, N. S., Dror, I., and Sadot, D., "Causes of atmospheric blur: comment on Atmospheric scattering effecton spatial resolution of imaging systems," Journal of the Optical Society of America A, 15(12), 3097-3106 (1998).

[14] Shamriz, S., Sasson, I., Dan, S., Itai, D., and Norman, S. K., "Prediction of overall atmospheric MTF with standard weather parameters: comparison with measurements with two imaging systems," 2471, 122-134 (1995).

[15] Bentz, B. Z., Redman, B. J., van der Laan, J. D., Westlake, K., Glen, A., Sanchez, A. L., and Wright, J. B., “Light transport with weak angular dependence in fog,” Optics Express, 29(9), 13231-13245 (2021).

[16] Michael, T. E., and Daniel, A. L., “Aerosol modulation transfer function model for passive long-range imaging over a nonuniform atmospheric path,” Optical Engineering, 52(4), 046201 (2013).

[17] Birch, G. C., Woo, B. L., Sanchez, A. L., and Knapp, H., “Image quality, meteorological optical range, and fog particulate number evaluation using the Sandia National Laboratories fog chamber,” Optical Engineering, 56(08), (2017).

[18] Corey, D. P., David, S. C., Will, H. C., Michael, C. R., and Raymond, A. S., "Measurement of optical blurring in a turbulent cloud chamber," 10002, 100020E (2016).

[19] Ishimaru, A., [Wave Propagation Scattering], (2005).

[20] Bohren, C. F., and Huffman, D. R., [Absorption and Scattering of Light by Small Particles] John Wiley & Sons Inc., (2004).

[21] Balanis, C. A., [Advanced Engineering Electrodynamics] John Wiley & Sons Inc., (2012).

[22] Pattyn, C. A., Zenker, J. P., Redman, B. J., Laan, J. D. v. d., Sanchez, A. L., Westlake, K., Patel, L., Bentz, B. Z., and Wright, J. B., “Influence of NaCl concentration on the optical scattering properties of water-based aerosols,” Applied Optics, (2023).

[23] Mätzler, C., “MATLAB functions for Mie scattering and absorption, version 2,” Institute for Applied Physics Research Reports, 8, 1 - 24 (2002).

[24] Bentz, B. Z., van der Laan, J. D., Glen, A., Pattyn, C. A., Redman, B. J., Sanchez, A. L., Westlake, K., Hastings, R. L., Webb, K. J., and Wright, J. B., "Detection and localization of objects hidden in fog," Proceedings of SPIE 11759 (2021).

[25] Beer, A., “Bestimmung der absorption des rothen lichts in farbigen flussigkeiten,” Annalen der Physik, 162, 78 - 88 (1852).

[26] Gallego, G., Delbrück, T., Orchard, G., Bartolozzi, C., Taba, B., Censi, A., Leutenegger, S., Davison, A. J., Conradt, J., Daniilidis, K., and Scaramuzza, D., “Event-Based Vision: A Survey,” IEEE Transactions on Pattern Analysis and Machine Intelligence, 44(1), 154-180 (2022).

[27] [Biases] Prophesee S.A., (2023).